MINISTRY OF EDUCATION AND TRAINING

VIETNAM ACADEMY OF SCIENCE AND TECHNOLOGY

GRADUATE UNIVERSITY OF SCIENCE AND TECHNOLOGY

DO THI THUY

SYNTHESIS OF GRAPHENE/POLYMER COMPOSITE FILM UTILIZING 3D PRINTING TECHNIQUE AND ORIENTED TO APPLICATION AS AN ELECTRODE MATERIAL

SUMMARY OF DISSERTATION ON CHEMISTRY

Code: 9 44 01 19

Ha Noi, 2023

The dissertation is completed at: Graduate University of Science and Technology, Vietnam Academy of Science and Technology

Supervisor: Associate Prof. Dr. Nguyen Tuan Dung
Prof. Dr. Tran Dai Lam

Referee 1:
Referee 2:
Referee 3:

The dissertation will be examined by Examination Board of Graduate University of Science and Technology, Vietnam Academy of Science and Technology at 9h00, 04 Dec. 2023

The dissertation can be found at:
- Graduate University of Science and Technology Library.
- National Library of Vietnam.

INTRODUCTION

1. The urgency of the thesis

Graphene, with its outstanding features, great electron dynamics, electrical conductivity, good thermal conductance, and large surface area... has attracted strong research interest in many fields, especially applications as an electrode material for energy storage components and electrochemical sensors [2]. The capacity value of the graphene electrode is much higher than that of other carbon materials, but theoretically, under ideal conditions with single-layer graphene and the entire surface used effectively, the maximum capacity is only 550 F/g. To increase the performance of the super condensers as well as improve the mechanical properties of the graphene membrane, the direction of research using graphene combination with polymer materials is thought to be a promising solution. On the other hand, polymer with its nature of organic material, soft, and flexible, will improve the machining capacity of graphene. In the field of electrochemical sensor manufacturing, electrodes based on composite graphene and polymer are also given special attention because they can combine the superior properties of both components. Compared to the use of pure graphene sensors, graphene/polymer composite sensors have prominent advantages such as flexibility and high selectivity, lightweight, and reasonable price.

Composite graphene/polymer is usually synthesized from solution and membrane by centrifugal rotation, drip coating, vapor condensation coincidence, or electrochemical flooding. These methods are often difficult because of the poor distribution of graphene in common solvents. In recent years, 3D printing technology has emerged and developed strongly, with applications in many different fields, especially in the manufacture of electronic components and electrochemical sensor manufacturing. 3D printing has made electrode design and manufacture much simpler, more accurate, and faster than traditional methods.

From the above analysis, the researchers chose the subject: "Study of composite graphene/polymer film manufacturing using 3D printing technology oriented to application as an electrode material".

2. Objectives of the thesis

Apply 3D printing techniques to make composite graphene with some polymer applications as electrode material in super condensers and electrochemical sensors.

3. Content of the thesis

- Fabrication of graphene composite 3D printing with polyvinyl alcohol using GO-based inks with ascorbic acid chemical detergent.

- Fabrication of graphene composite 3D printing with polyacrylic acid using GO-based inks with UV agents.

- Fabrication of composite 3D printing of graphene with electrically conductive polymers (polyaniline, poly(1,8-diaminonaphtalen)) using GO-based inks with electrochemical method.

- Evaluate the application of composite graphene/polymer 3D printing materials as electrodes in supercapacitors and electrochemical sensors.

4. Layout of the thesis

The thesis comprises 120 pages, with 55 figures,14 tables, and a bibliography of 120 references. The structure of the thesis follows a typical layout, which includes an introduction, three content chapters, and a conclusion. Notably, the novelty of the research has resulted in the publication of eight papers, with two papers listed in SCIE journals and two in Scopus-indexed journals, as well as two papers listed in specialty national journals.

CHAPTER 1. OVERVIEW

Chapter 1 is presented in 32 pages including 18 pictures introducing graphene, graphene/polymer composite, and the research situation of applying 3D printing technique in manufacturing graphene/polymer composite electrodes.

3D printing technology or gradual manufacturing technology is the process of sampling from a digital model that is carried out automatically through a 3D printer. The object was created exactly according to the design pattern. Graphene with high electron dynamics, electrical conductivity, good thermal conduction, large private surface area... It's fascinating that scientists are working on electrodes with a variety of applications, including super condensers and electrochemical sensors. Polymer is a soft, flexible material with good adhesion. The combination of graphene and polymer gives the graphene/polymer composite many unique properties. The field of composite graphene/polymer electrodes is attractive to scientists.

CHAPTER 2. EXPERIMENTAL

Chapter 2 is presented in 12 pages, 4 figures which include:

2.1. Materials

2.2. Experimental method

2.2.1. Synthesis of graphene oxide

2.2.2. Synthesis of composite reduction graphene oxide (rGO) with polyvinyl alcohol (PVA) using reduction ascorbic acid

2.2.3. Synthesis of rGO composite 3D printing film with polyacrylic acid using UV irradiation

2.2.4. Synthesis of rGO composite 3D printing film with polyaniline modified nano MnO_2 using as supercapacitor

2.2.5. Synthesis of rGO composite 3D printing film with poly(1,8-diaminonaphthalene) modified nano Ag using as sensor

CHAPTER 3. RESULTS AND DISCUSSION

Chapter 3 is presented in 55 pages which includes:

3.1. Study on the manufacture of graphene oxide ink

3.1.1. Characteristics of GO

GO determines characteristic properties using the following techniques: transform infrared spectrum (FT-IR), Raman spectrum, X-ray diffraction spectrum (XRD), and Field Emission Scanning Electron Microscopy (FE-SEM).

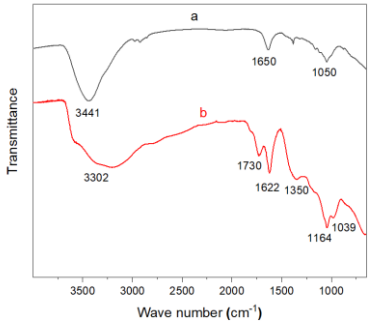

Fig. 3.1. FT-IR of graphite (a) and GO (b)

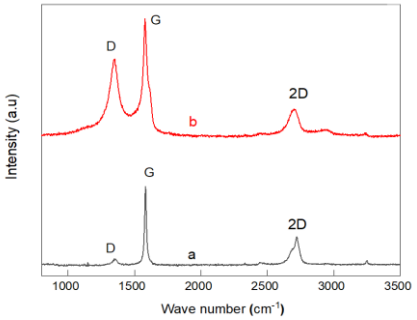

Fig. 3.2. Raman spectrum of graphite (a) và GO (b)

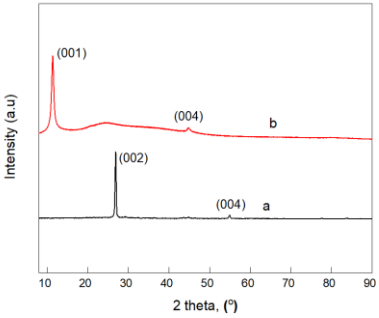

Fig.3.3. XRD patterns of graphite (a) và GO (b)

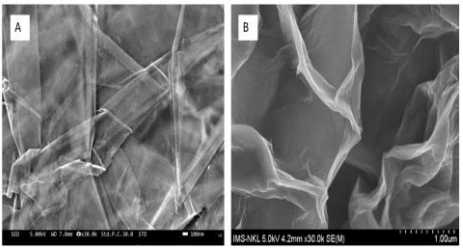

Fig.3.4. FE-SEM images of graphite (A) và GO (B)

The results show that GO is synthesized successfully from graphite by chemical methods. GO is thin, with a lot of space in the middle. The oxidation process separated the graphene layers in the graphite structure.

3.1.2. Properties of GO Ink

3.1.2.1. Viscosity of GO ink

The concentration of GO ink in the thesis was chosen at 8 mg/mL corresponding to a dynamic viscosity of 30.6 mPa.s.

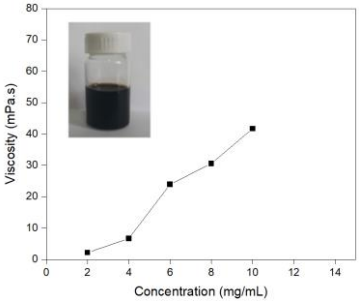

Fig. 3.5. Dynamic viscosity of GO ink at 25ºC

3.1.2.2. Zeta potential of GO ink

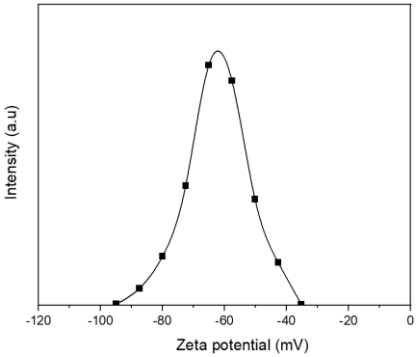

Hình 3.6. Zeta potential of GO ink

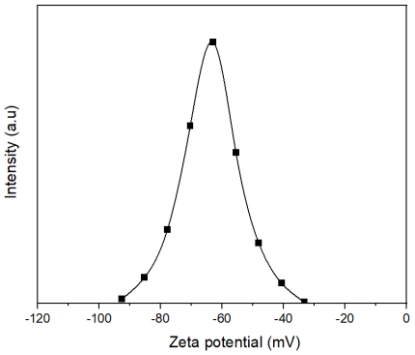

Hình 3.7. Zeta potential of GO ink after two months

GO

The zeta potential of the GO measurement was -65 mV; after two months, this value of zeta reached -63 mV, demonstrating the stability of the ink.

3.2. Synthesis of a 3D composite graphene oxide compound with a non-conductive polymer

3.2.1. Synthesis of rGO/PVA composite film using ascorbic acid

3.2.1.1. Effect of ascorbic acid

Composite film made of GO, ascorbic acid, and PVA (PVA makes up 10% of the wt. compared to GO) and different amounts of ascorbic acid (5, 10, and 15% wt.).

The obtained CV curve has a sharp oxidation-reduction peak with a much higher current intensity when ascorbic acid is present. The ascorbic acid level, specially selected, is 10% by weight (fig.3.8)

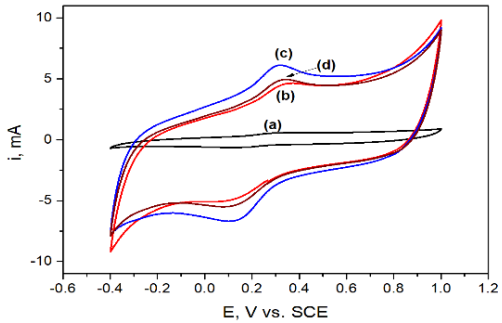

Fig. 3.8. The results of CV measurement in $K_3[Fe(CN)_6]/K_4[Fe(CN)_6]$ solution of GO (a) membrane and GO/PVA composite with different content of ascorbic acid: 5% (b), 10% (c), 15% wt. (d)

3.2.1.2. PVA content

Zeta potential results

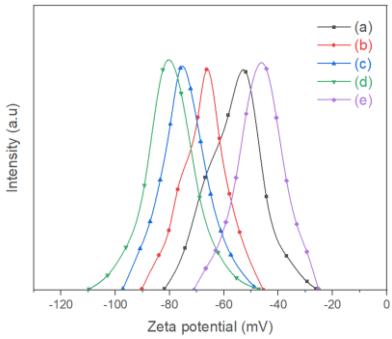

Fig. 3.9. The zeta potential results of GO-ascorbic acid-PVA ink with the content of PVA: 0% (a); 5% (b); 10% (c); 15% (d), 20% wt (e)

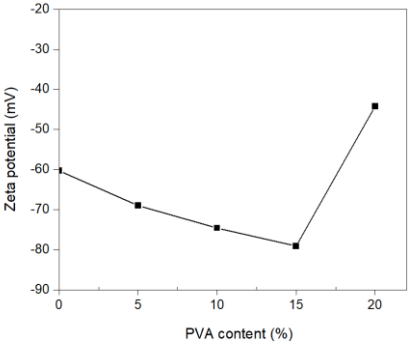

Fig. 3.10. The relationship between zeta potential and PVA content

In the case of PVA, which occupies 5% wt., the value of the zeta potential is 69 mV. PVA content is 15% wt., and the zeta value reaches 79.1 mV. This value ensures good electrostatic propulsion between the adhesive particles and high stability of the ink. Continuing to increase the PVA, the value of the zeta potential tends to decrease, and the stability of the ink also decreases.

The electrochemical

The results show that the current intensity increases with the PVA content increasing from 5 to 15% wt., but is slightly reduced in the case of

20% PVA wt. However, in the case of higher PVA levels (20% wt.), the observed current intensity is lower than the other samples; this is due to the low content of rGO in the printed film. PVA content of 15% wt. is selected for subsequent experiments (fig.3.11)

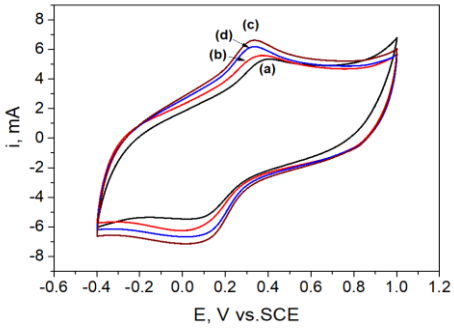

Fig. 3.11. The result of CV in $K_3[Fe(CN)_6]/K_4[Fe(CN)_6]$ 5 mM solution of rGO/PVA with content PVA of 5% (a), 10% (b), 15% (c), 20% wt. (d)

3.2.1.3. Characterization of composite GO/ascorbic acid/PVA

Morphology

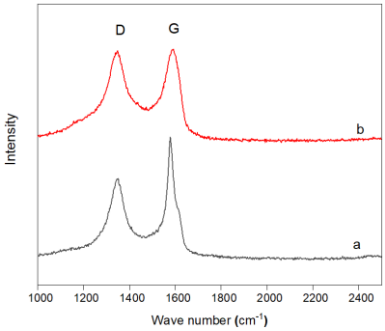

Fig 3.12. Raman spectra of GO (a) and rGO/PVA (b)

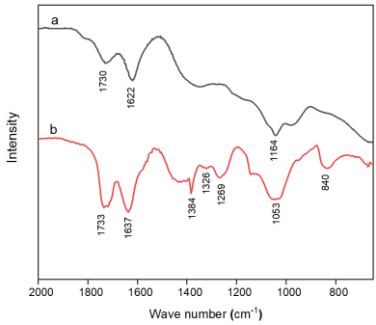

Fig 3.13. FT-IR spectra of GO (a) and rGO/PVA (b)

Raman spectrum results show the characteristic peaks of graphene: peak D at 1350 cm^{-1} and peak G at 1588 cm^{-1}. The increased I_D/I_G ratio (from 0.86 to 1.02) indicates that GO has been reduced into rGO.

On the FT-IR spectrum of the composite rGO/PVA, the absorption peak at 1384 cm^{-1} corresponds to C-O-H bond, the pic at 1326 cm^{-1} corresponds to CH/CH2 bonds, the peak at 1269 and 1053, the 840 cm^{-1}, corresponds to C- O-C bonds and C=O, C-C. The absorption peaks at 1733 cm^{-1} and 1637 cm^{-1} correspond to the stretch vibrance C=O and C=C bonds of both PVA and rGO.

Electrochemical

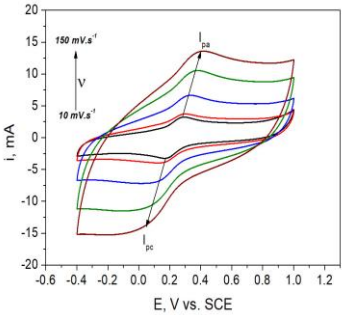

Fig. 3.15. The CV result of rGO/PVA in $K_3[Fe(CN)_6]$/ $K_4[Fe(CN)_6]$ 5 mM solution

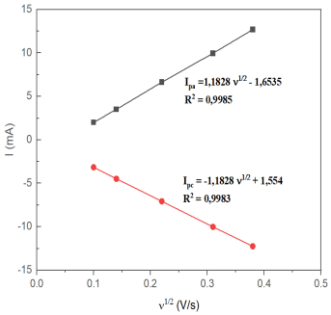

Fig. 3.16. A straight line between I_{pa}, I_{pc}, and the square root of the scan rate

The rGO/PVA electrode has an effective area of 0.32 cm^2, which is equivalent to one-third of its geometric area. The utilization of 10% weight ascorbic acid in the process of reduction GO is not highly efficient.

3.2.1.4. Capacity performance of composite GO/ascorbic acid/PVA film

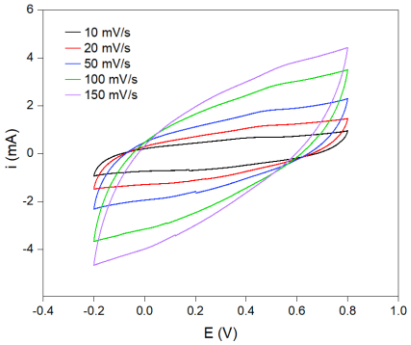

Fig 3.16. The CV result of composite rGO/PVA film in H_2SO_4 1 M solution, scan rate from 10 to 150 mV/s

Table 3.3. The specific capacity performance of composite rGO/PVA

Scan rate (mV/s)	10	20	50	100	150
Specific capacity (F/g)	92	88	75	70	65

The CV of the GO/ascorbic acid/PVA film at low scanning speed has a deformed rectangular shape, characteristic of a double condenser with a relatively high voltage resistance.

3.2.2. Synthesis composite rGO/PAA using UV irradiation

3.2.2.1. Zeta potential of GO/AA ink

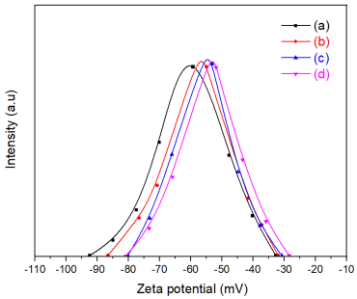

Fig. 3.18. Zeta potential of GO/AA with AA content: 5% (a), 10% (b), 15% (c), 20% wt.(d)

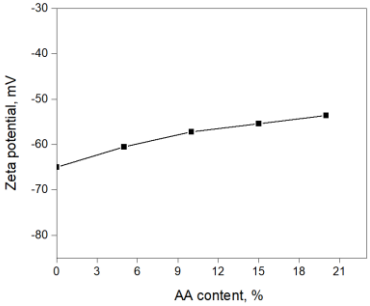

Fig 3.19. The dependence of zeta potential on AA content

The zeta potential analysis indicates that AA comprises 5 to 20% by weight, confirming the stability of the ink and the GO particles do not tend to merge.

3.2.2.2. Effect of UV irradiation time

The GO/AA composite film is manufactured using 3D printing and then exposed to UV radiation in varying intervals of 1.2, 3.6, and 6 seconds.

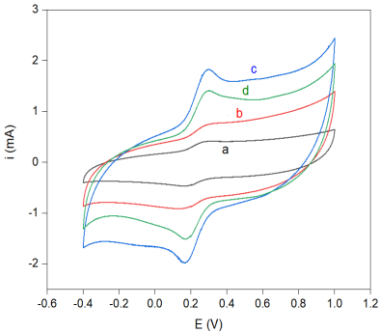

Fig. 3.20. The CV result of GO/AA film with time irradiation of UV: 0 seconds (a); 1.2 seconds (b); 3.6 seconds (c) and 6 seconds (d)

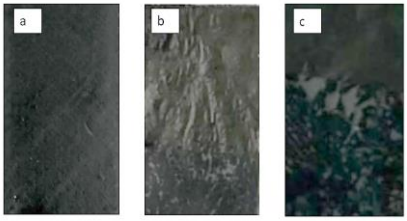

Fig 3.21. Image of GO/AA composite film after UV exposure 3.6 seconds (a), 6 seconds (b) and GO film after 3,6 seconds (c)

Table 3.4. The value of I_{pa}, I_{pc}, ΔE_p with UV irradiation from 0÷6 seconds

Time (seconds)	**I_{pa} (mA)**	**I_{pc} (mA)**	**ΔE_p (V)**
0	0.65	-0.78	0.31
1.2	0.72	-0.88	0.13
3.6	1.89	-2.01	0.12
6	1.39	-1.50	0.12

The rGO/PAA composite has the best electrochemical activity with a radiation projection time of 3.6 seconds. AA improves the adhesion of rGO.

Effect of AA content

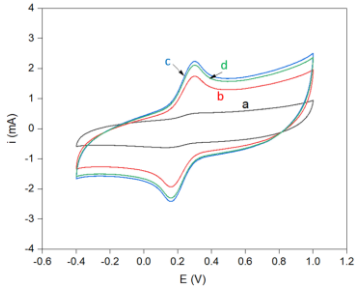

Fig 3.22. The results of CV in $K_3[Fe(CN)_6]/K_4[Fe(CN)_6]$ 5 mM solution rGO/PAA with AA content: 0% (a), 5% (b), 10% (c), 15% (d)

With the presence of AA accounting for 10% wt., the obtained CV curve shows a sharp oxidation-reduction peak and current intensity increases strongly.

3.2.3. Characteristics and properties of rGO/PAA composite film

Characterization

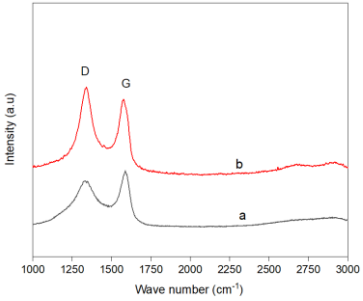

Fig 3.23. Raman spectra of GO/AA (a) and rGO/PAA (b)

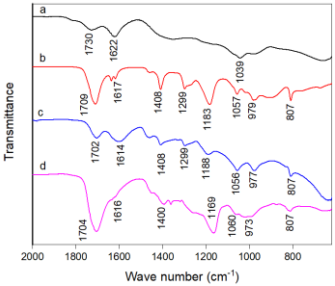

Fig 3.24. IR spectra of: GO (a), AA (b), GO/AA (c), rGO/PAA (d)

The Raman spectra indicated that the (ID/IG) ratio of rGO/PAA was

1.18, which was higher than the ratio of GO/AA, which was 0.86. This suggests that the reduction of GO had occurred.

The FT-IR spectra of the composite rGO/PAA show a shift of the peak at 1614 cm^{-1}, which is characteristic of the C=C bond in the monomer, to 1616 cm^{-1}. Additionally, the strength of the peak has significantly decreased. The presence of a peak at 1188 cm^{-1} was related to the C-C stretching vibrations. This peak changed to 1169 cm^{-1} and exhibited a significant rise in intensity, indicating the taking place of the PAA polymerization process.

Table 3.6. Components of GO/ AA và rGO/PAA

Sample	Element	% Atomic	% Weight
GO/AA	C	54.23	58.14
	O	45.77	41.86
rGO/PAA	C	65.25	69.83
	O	34.75	30.17

The results demonstrated that UV irradiation effectively decreased the %O mass ratio on the surface of the GO/AA film from 41.86% to 30.1%, showing evidence of the successful reduction process of GO.

Electrochemical

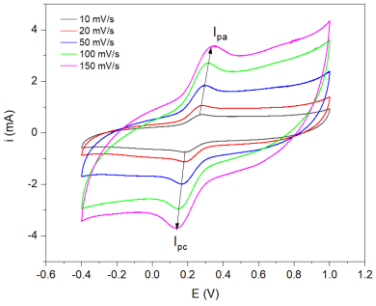

Fig 3.26. The CV results of rGO/PAA composite film

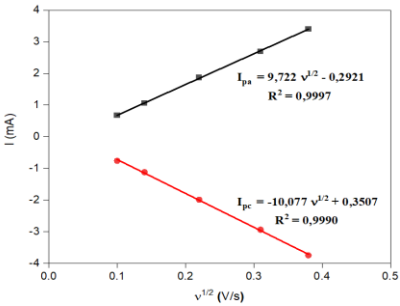

Fig 3.27. A straight line between I_{pa}, I_{pc}, and a square root of the scan rate

The effective area of the rGO/PAA composite electrode is 1.30 cm^2, which is higher than 1.3 times the geometric area, demonstrating that UV radiation has an effective reduction.

3.2.4. Capacitive performance of rGO/PAA composite film

The capacitive performance of rGO/PVA was evaluated by the cycle voltammetry (CV) method in 1 M H SO solutions, with a voltage range of -0.4 ÷ +1.0 V, a scanning speed of 10 ÷ 150 mV/s and galvanostatic charge/discharge (GCD) techniques with a current density of 1 ÷ 5 A/g.

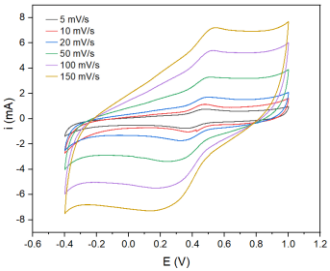

Fig 3.28. CV curves of rGO/PAA in 1 M H_2SO_4 solution

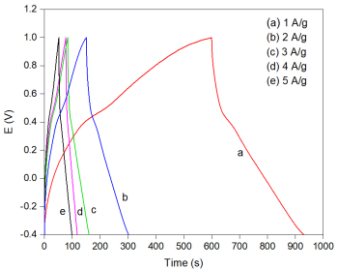

Fig 3.29. GCD curves of rGO/PAA in 1 M H_2SO_4 solution

Table 3.7. The specific capacitance (C_s) of rGO/PAA depends on a scan rate

Scan rate *(mV/s)*	5	10	20	50	100	150
C_s ***(F/g)***	320	205	192	189	175	150

The specific capacitance decrease with increasing scanning rate can be explained by the limitation of the diffusion of the ions in the electrolyte solution to the pore of the electrode material. When the scanning rate is low, the ions in the electrolyte diffuse across into most of the holes, and the exchange of electrons between the electrolyte and the electrodes takes place at many sites. As the scan rate increases, the process slows down, leading to a reduction in the sample capacity.

Table 3.8. The specific capacitance of rGO/PAA at different current densities

Current density (A/g)	1	2	3	4	5
Specific capacitance (F/g)	321	285	260	196	175

The GCD curves of the rGO/PAA composite are typical of both double-layer supercapacitors and pseudocapacitors. The linear line indicates double-layer supercapacitors, while the non-linear line represents pseudocapacitors. The cyclic stability was investigated at a current density of 5 A/g for 5000 cycles. The results show a capacitance retention of 82%.

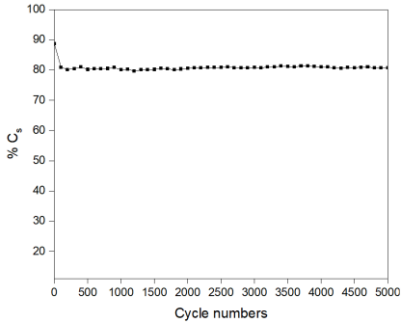

Fig.3.30. Decrease of C_s of rGO/PAA composite at current density of 5 A/g

3.3. Synthesis of composite graphene printing film with electrically conductive polymer

3.3.1. Synthesis rGO/PANi composite film modified MnO_2 nano

3.3.1.1. Property of in GO/ANi ink

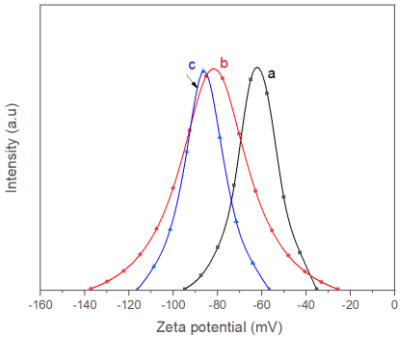

Fig 3.31. Zeta potential results of GO:ANi =1:0 (a), 2:1 (b), 1:1 (c)

For the GO: ANi ratio of 1:1, the absolute zeta value measured is 86.1 mV, indicating effective electrostatic interaction between the adhesive particles. Because print ink has high stability, ANi has a role to play in increasing stability for print ink.

3.3.1.2. Synthesis rGO/PANi composite film decorated MnO_2 nano

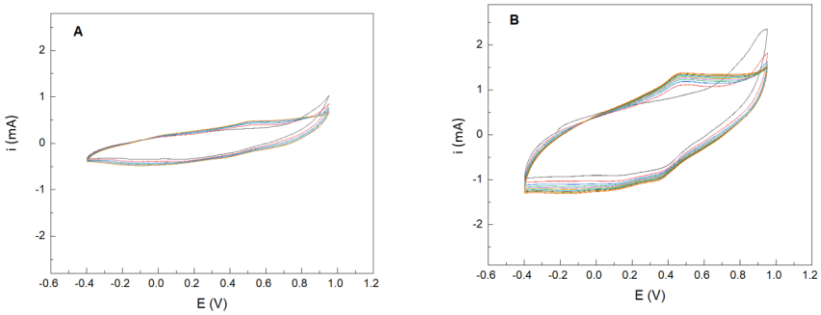

Fig 3.33. CV curves of GO/ANi: A) without reduction GO, B) reduction GO.

The results indicated that applying a voltage of -0.8 V resulted in the reduction of GO, leading to the formation of more electrically conductive rGO. Additionally, the electrochemical polymeration of PANi was shown to be beneficial.

Time of reduction GO

For a reduction period of 40 seconds, there is a slight rise in the current intensity value compared to 30 seconds. Therefore, a condition of 30 seconds

is chosen for further investigation (Fig 3.34)

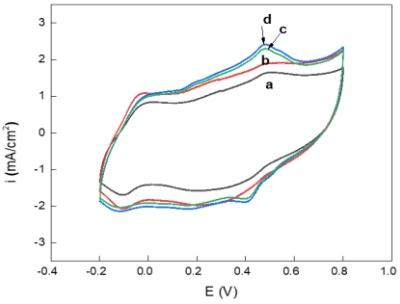

Fig 3.34. CV result of rGO/PANi in 1 M H_2SO_4 solution with reduction of GO: 10 (a), 20 (b), 30 (c), 40 seconds (d)

The ratio of GO:ANi

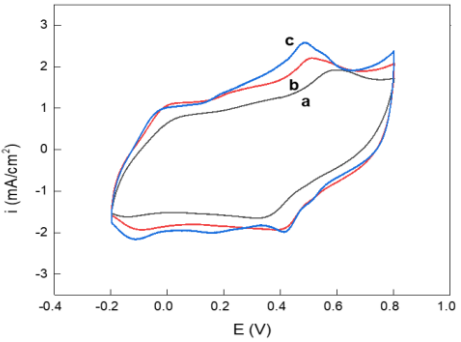

Fig 3.35. CV result in 1 M H_2SO_4 solution, scan rate 50 mV/s of composite rGO/PANi with ratio of GO:ANi is 2:1 (a), 1:1 (b), 1:2 (c)

The CV study results clearly showed the influence of PANi in the composite material. As the ANi ratio grew, the strength of the oxidation current also increased. Consequently, a GO:ANi ratio of 50% was chosen.

Time of electrodeposition MnO_2

In this work, the printed rGO/PANi film was doped with MnO_2 nanoparticles by electrodeposition in an aqueous solution containing 50 mM $MnSO_4$, 0.2 M H_2SO_4, and 0.5 M KCl as electrolytes. A potential of +0.6 V was applied to the rGO/PANi working electrode within 200 s, and Mn^{2+} ions were oxidized to form MnO_2 and deposited on the rGO/PANi surface. These electrochemical conditions were selected so that PANi can exhibit good electric conduction and the obtained MnO_2 nanoparticles could have better capacitive properties (Fig. 3.36).

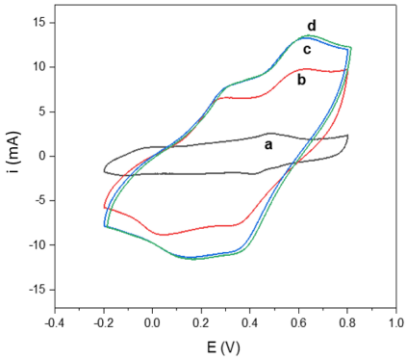

Fig 3.36. CV result of rGO/PANi (a) and rGO/PANi/MnO_2 with different time applied of 100 (b); 200 (c) và 300 second (d)

3.3.1.3 Characterization properties of rGO/PANi/MnO_2 composite film

Raman spectra

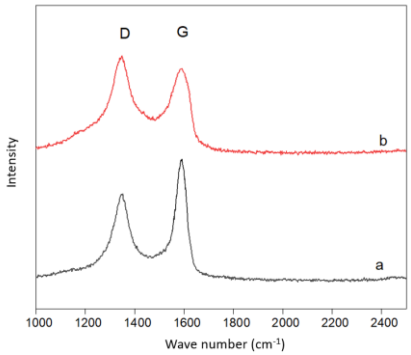

Fig 3.37. Raman spectra of GO/ANi (a) and rGO/PANi/MnO_2 (b) composite

As can be seen from Fig. 3.37, the typical peaks of graphene, peak D is at 1344 cm^{-1}, and peak G is at 1588 cm^{-1}. The relative strength ratio of peak D and peak G (I_D/I_G) of rGO/PANi/MnO_2 is 1.20, indicating that GO has been reduced into rGO.

FT-IR spectra

FT-IR spectrum of rGO/PANi/MnO_2 film represents the characteristic absorption bands of PANi: the peak at 1609 cm^{-1} is now shifted to 1626 cm^{-1}, corresponding to the quinoid structure of PANi (N=Q=N stretch), the novel peak at 3357 cm^{-1} is associated with N-H stretching vibration. It is appeared also strong bands at 1164 cm^{-1} and 873 cm^{-1} due to the C-H bending in the plan and out of the plan, respectively. Aniline has been well electropolymerized to form PANi (Fig 3.38)

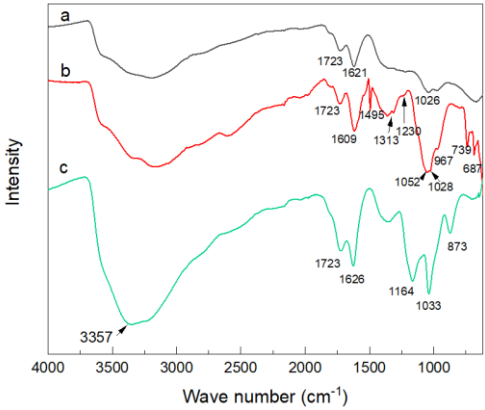

Fig 3.38. FT-IR spectra of GO (a), GO/ANi (b), rGO/PANi/MnO_2 (c)

EDX spectra

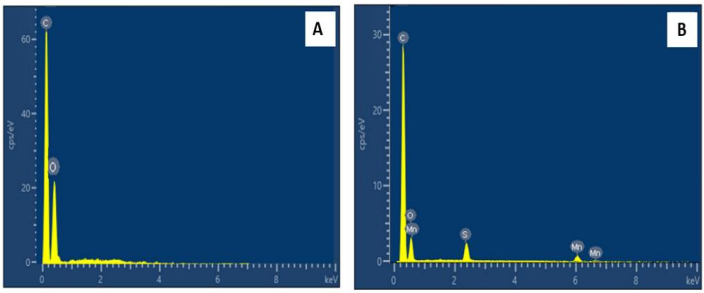

Fig 3.39. EDX spectra of rGO/PANi (A), rGO/PANi/MnO_2 (B)

Table 3.9. Element composition of rGO/PANi and rGO/PANi/MnO_2

Sample	Element	% Atomic	% Weight
rGO/PANi	C	79.45	85.54
	O	20.55	14.36
rGO/PANi/MnO_2	C	73.01	79.78
	O	23.18	19.02
	Mn	2.09	0.70
	S	1.72	0.50

The results presented in Table 3.9 indicate that rGO/PANi composite film, mostly composed of 79.45% C and 20.55% O, does not exhibit the presence of N, likely due to the low nitrogen content. The composite film rGO/PANi/MnO_2 consists of C (73.11%), O (23.18%), and a small amount of sulfur impurities (1.72%) originating from the composite film synthesis in

an H_2SO_4 solution. The existence of Mn (2.09%) is confirmed by the EDX spectrum (Figure 3.40), which exhibits extinction peaks at 5.9 eV and 6.5 keV. Therefore, the deposition of MnO_2 crystals onto the surface of the rGO/PANi film was successful.

XPS spectra

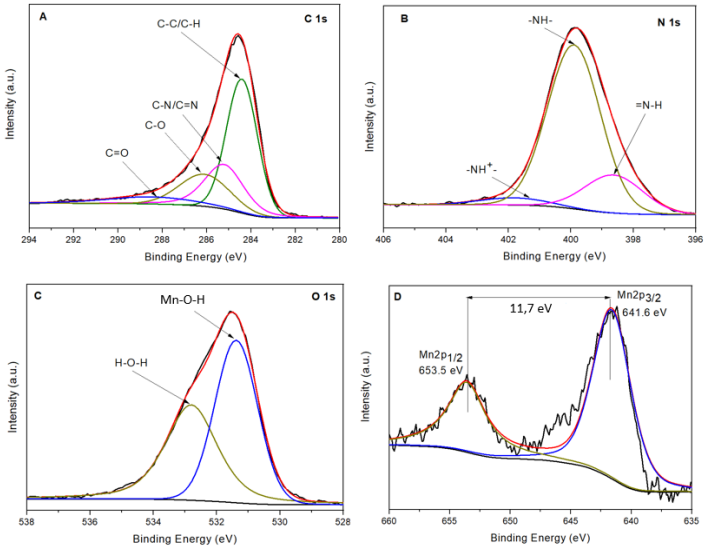

Fig 3.41. XPS spectra of C 1s(A), N 1s (B), O 1s (C) và Mn 2p (D)

To investigate the chemical composition and chemical states of various elements in the composites, XPS analysis was performed. The spectrum in Fig. 3.41 reveals the existence of C, N, O, and Mn in the composite (Figure 3.41A). The XPS N1s spectrum is divided into three peaks (Figure 3.41B): the most significant peak occurs at 399.5 eV and corresponds to the −NH− bond (benzenoid amine), the peak with a lower intensity at 398.9 eV represents the =NH− bond (quinoid imine), and a peak is observed at a higher binding energy of 401.7 eV, indicating the presence of the $-NH^+-$ bond, which suggests that some N atoms have been protonated to N^+. This demonstrates the successful electrochemical polymerization of PANi from ANi. The XPS of the O 1s (Figure 3.41C) shows two distinct peaks at 531.4 and 532.8 eV, indicating the presence of Mn−O−H and H−O−H bonds. Figure 3.41D displays the XPS Mn 2p spectrum, which has two peaks at energy levels of 653.5 and 641.8 eV, corresponding to the $2p_{1/2}$ and $2p_{3/2}$ states, respectively. The spin energy separation of 11.7 eV confirms the presence of Mn^{+4} (MnO_2) in the composites.

3.3.1.4. Capacity performance of rGO/PANi/MnO_2 study

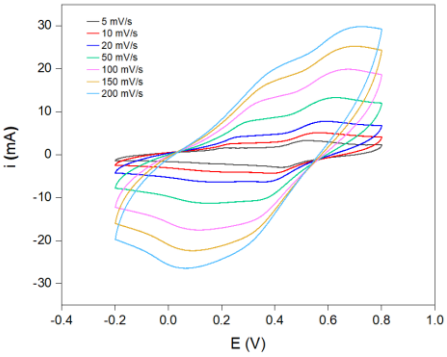

Fig 3.42. CV results of rGO/PANi/MnO_2 with the different scan rate

Table 3.10. Specific capacitance (C_s) of rGO/PANi/MnO_2 with scan rate from 5÷200 mV/s

Scan rate (mV/s)	5	10	20	50	100	150	200
C_s (F/g)	680	600	550	490	420	380	325

The composite electrode rGO/PANi/MnO_2 exhibits a capacitance of 680 F/g when the scanning speed is 5 mV/s, and a capacitance of 385 F/g when the scanning speed is increased to 200 mV/s. As the scanning speed increases, the capacity declines due to the decreased diffusion of the H^+ ion.

The capacity property of rGO/PANi/MnO_2 electrode and rGO/PANi electrode was also studied by the GCD method with a current density of 1÷10 A/g.

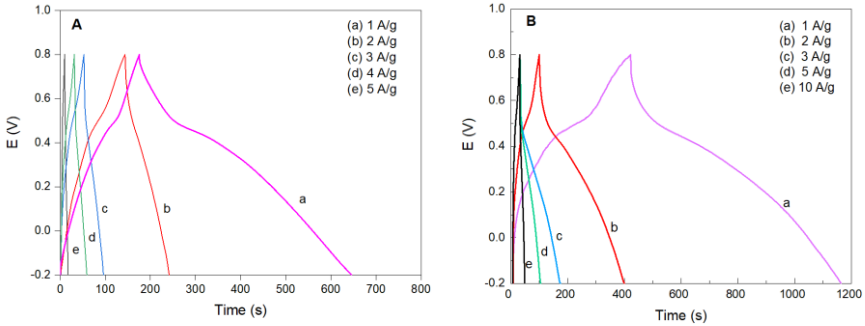

Fig 3.43. The charging and discharging curves of GO/PANi (A) and rGO/PANi/MnO_2 (B) composite in different current density

Table 3.11. The specific capacitance of rGO/PANi and rGO/PANi//MnO_2 composites at a current density of 1÷ 10 A/g

Current density (A/g)	1	2	3	5	10
C_s (F/g) rGO/PANi	450	390	320	295	270
C_s(F/g) rGO/PANi/MnO_2	740	680	600	495	420

The strength of the rGO/PANi/MnO_2 electrodes is investigated through a specific capacity decrease in charge-discharge cycles at a 15 A/g current density, as shown in Fig 3.44.

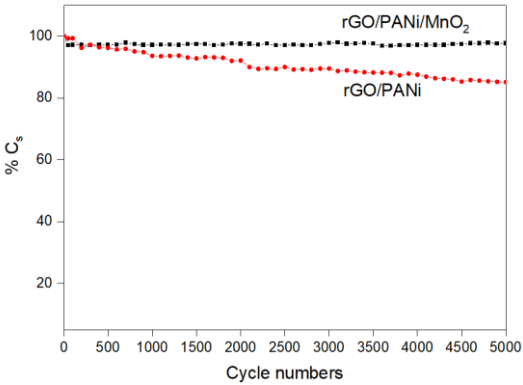

Fig 3.44. Cyclic stability of the rGO/PANi/MnO_2 (a) and rGO/PANi (b) composite at a current density of 15 A/g

After 5000 charge-discharge cycles, the rGO/PANi/MnO_2 composite electrode still maintains 97% C_s, while the rGO/PANi electrode only retains 85% C_s.

3.3.2. Fabrication of graphene/P(1,8-DAN) modified AgNPS

3.3.2.1. Fabrication of rGO/P(1,8-DAN)/Ag NPS composite

In this thesis, GO and (1,8-DAN) inks are used to create a layer-by-layer GO/(1,8-DAN) composite film on a 3D printing. The GO/(1,8-DAN) electrodes were treated electrochemically in the droplet of a solution containing 1 M $HClO_4$ and 0.1 M $LiClO_4$ to reduce GO by chronoamperometry method at − 0.8 V (vs. SCE) in 30 s). Next, polymerization of 1,8-DAN is carried out by cyclic voltammetry technique within the potential range from -0.15 V to +0.95 V (vs. SCE) with a scan rate of 50 mV/s for 10 cycles.

CV results show that P(1,8-DAN) was polymerization successful.

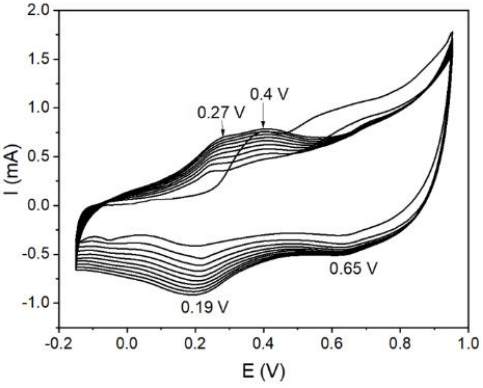

Hình 3.46. CV result synthesis P(1,8-DAN) in 1 M $HClO_4$ and 0.1 M $LiClO_4$ solution

3.3.2.2. Characterization of GO/P(1,8-DAN)/AgNPS composite film

Electrochemical

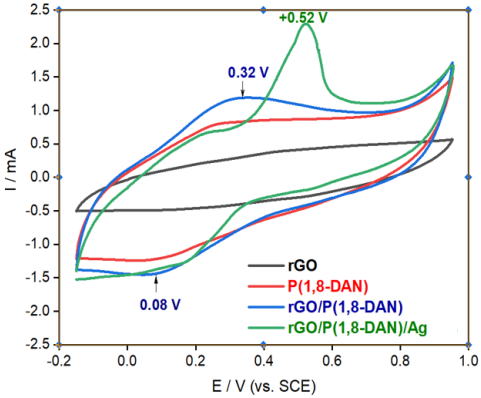

Fig 3.47. CV results in 0.1 M $HClO_4$ of: rGO (a), P(1,8-DAN) (b), rGO/P(1,8-DAN) (c) and rGO/P(1,8-DAN)/AgNPS (d)

The CV analysis of the rGO/P(1,8-DAN)/AgNPS composite exhibited a strong peak at +0.52 V, indicating the oxidation reaction of Ag^o. Therefore, when the voltage is applied to -0.3 V for 30 seconds, the Ag^+ ion has been absorbed with P(1,8-DAN) and is reduced into Ag^o.

Morphology

It can be seen that on the surface of the electrode appeared small white dots, spherical shapes with sizes between 30 and 50 nm uniform dispersion across the surface composite matrix, and without agglomeration (Fig.3.48).

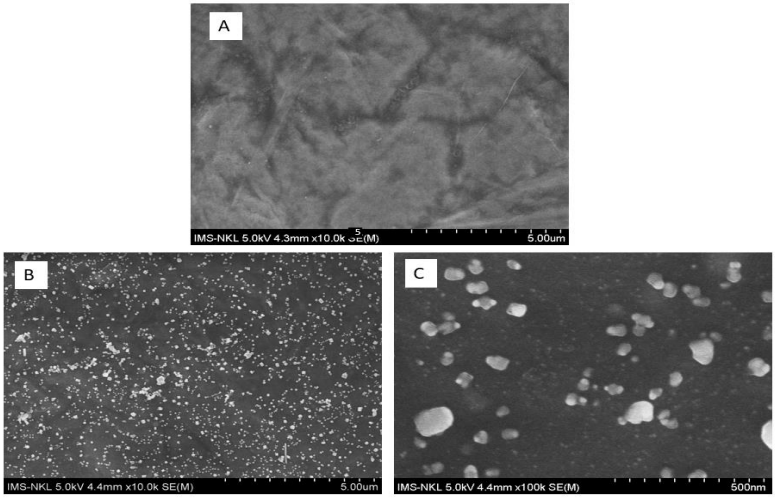

Fig 3.48. FE-SEM image surface of GO (A), rGO/P(1,8-DAN) (B) and rGO/P(1,8-DAN)/AgNPS (C)

EDX spectra

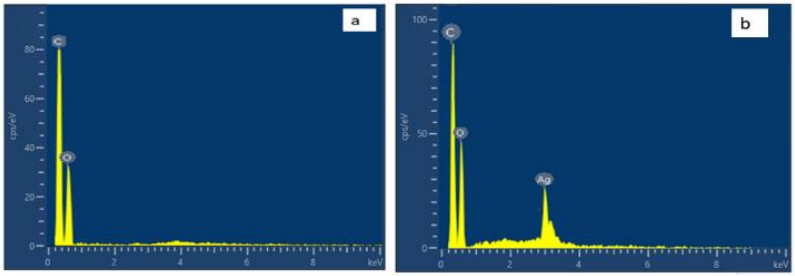

Fig 3.49. EDX spectra of rGO/P(1,8-DAN) (a) and rGO/P(1,8-DAN)/AgNPS (b) composite film

Table 3.12. Element composition of rGO/P(1,8-DAN) and rGO/P(1,8-DAN)/AgNPS composite film

Sample	Element	% Weight	% Atomic
rGO/P(1,8-DAN)	C	52.71	62.96
	O	47.29	37.04
rGO/P(1,8DAN)/Ag	C	50.95	60.23
	O	42.72	38.92
	Ag	6.33	0.85

The EDX spectrum analysis shows that the rGO/P(1,8-DAN)/Ag

composite film is mostly made up of C (50.95%) and O (42.72%). EDX also indicated the presence of Ag (6.33%), with a peak appearing at 3.1 keV. Thus, the deposition of AgNPS on the surface of the rGO/P(1,8-DAN) membrane has been successfully carried out.

XPS spectra

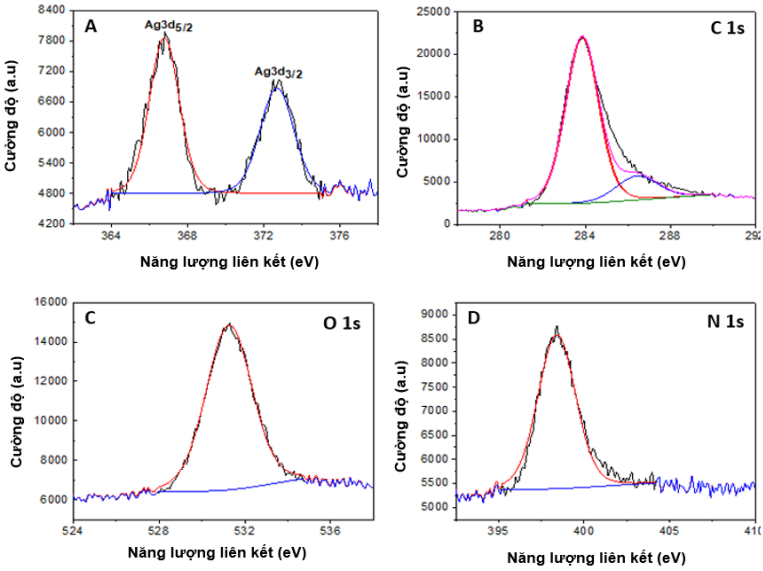

Fig 3.50. XPS spectra of Ag 3d (A), C 1s (B), O 1s (C) và N 1s (D)

The presence of symmetrical peaks located at 366.7 and 372.7 eV are attributed to the binding energies for Ag 3d that correspond to the binding points of spin–orbit for Ag 3d (5/2) and Ag 3d (3/2) levels (Fig. 3.50A). The energy splitting value of the Ag 3d is 6.0 eV, signifying the formation of metallic silver on the rGO/P(1,8-DAN) surface. Compared with the standard binding energies for pure silver, which are 368.1 and 374.1 eV, the shift of both Ag 3d5/2 and Ag 3d3/2 to the lower binding energy may be due to the occurrence of electron transfer between AgNPs and the P(1,8-DAN) polymer chain. Fig. 3.50B shows XPS spectrum of C1s could be curve-fitted with two peaks, with binding energy at 284.0 eV corresponding to the bond C-C/C=C in the aromatic rings and 286.4 eV for C=O/O–C–O species of rGO/P(1,8-DAN) composite. The O1s spectrum peak (Fig. 3.50C) with a binding energy of 531.5 eV and the N1s spectrum peak (Fig. 3.50D) with a binding energy of 398.4 eV assigned to the bond Ag-O and the oxygen binding in the graphene oxide, and the stronger interaction of AgNPs with an amino group of P(1,8-DAN), respectively.

3.3.2.3. Detection of cefepime antibiotics

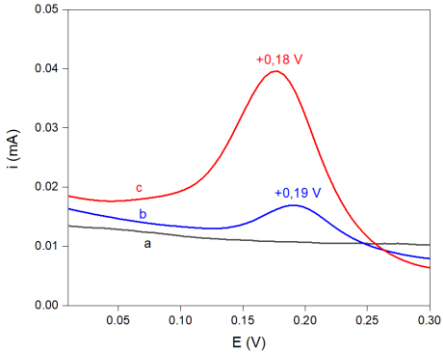

Hình 3.51 DPVs obtained in 0.1 M PB solution (pH 7.4) in the absence and presence of 2.0 µM cefepime antibiotic based on rGO/P(1,8-DAN) and rGO/P(1,8-DAN)/AgNPs

The result in Figure 3.51 shows that without cefepime, the DPV does not appear (line a). In the case of cefepime, a clear oxidation peak appears at +0.19 V (for rGO/P(1,8-DAN), line b) and +0.18 V (for rGO/P(1,8-DAN)/AgNPS, line c). The peak intensity of rGO/P(1,8-DAN)/AgNPS electrode is 2.3 times higher than rGO/P(1,8-DAN) electrode. After being decorated with AgNPS, the oxidation peak of the composite film has shifted toward negative over 0.01 V due to the increased surface area of the membrane.

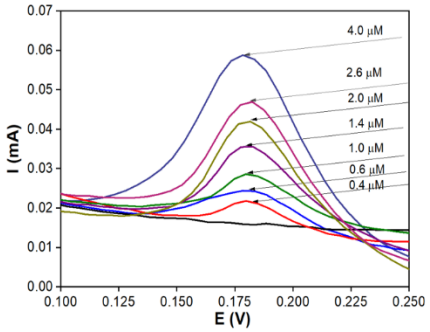

Fig 3.52. The DPV responses of rGO/P(1,8-DAN)/AgNPs electrodes in 0.1 M PBS solution containing various concentrations of cefepime antibiotics from 0.4÷4.0 µM

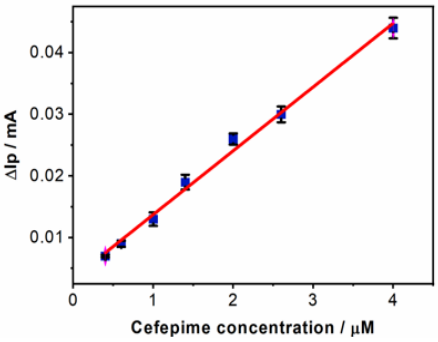

Fig 3.53. The corresponding plot of current peak height vs. cefepime concentration.

A linear correlation between current peak heights and the cefepime was

described by the below linear regression equations: $\triangle I_p$ (mA) = 0.0104 X $C_{cefepime}$ (µM) + 0.0034 with R^2 = 0.9935.

The limit of detection (LOD) was 0.08 µM

Reproducibility and stability

Evaluation of the reproducibility was based on six repeated measurements of the DPV electrochemical signals of 2.0 µM cefepime in PB solution (pH 7.4). The precision of the relative standard deviation (RSD) was 2.20%.

The long-term stability of the 3D-printed rGO/P(1,8-DAN)/AgNPs sensor was tested by measuring DPV peak height of 2.0 µM cefepime in PB solution for 26 days (Fig. 3.54).

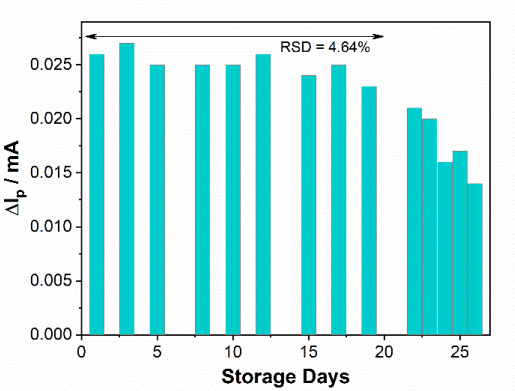

Fig 3.54. Evaluating the long-time stability of 3D-printed rGO/P(1,8-DAN)/AgNPs between 1 and 26 storage days on 2.0 µM cefepime

It was found that the DPV peak height remains at 91% of its initial value with a relative standard deviation of less than 4.7% after 19 days. This result indicates the suitable stability of the proposed modified electrode.

Cefepime assay in real samples

Bảng 3.15. Results for the determination of cefepime in commercial pharmaceutical

Sample	Found content (g)	Recovery	RSD (%)
Verapime 1 g	0,971	97,1	1,09
Cefeme 0,5 g	0,560	112,0	5,29
Cefeme 1g	0,948	94,8	1,62

The data summarized in Table 3.15 show that the recovery of the pharmaceutical samples was between 94.8 and 112% with RSDs from 1.09 to 5.29%.

CONCLUSION

1. Graphene oxide (GO) was synthesized from graphite using a chemical method and subsequently used as ink for 3D printing. The viscosity indicates that the optimal concentration of GO for printing ink is 8 mg/mL. The zeta potential of -65 mV exhibited the excellent stability of the ink.

2. The film for 3D printing is made of a composite material consisting of rGO and polyvinyl alcohol (PVA), and ascorbic acid is used as a reduction. When using a ratio of GO:ascorbic acid:PVA = 100:10:15, the composite film exhibits the highest electrochemical activity, but it is not significantly high. Additionally, the effective area of the electrode is only 32%. The specific capacity value (Cs) of the rGO/ PVA film in a 1 M H_2SO_4 solution reaches 92 F/g at a current density of 1 A/g.

3. The film for 3D printing is made of a composite material consisting of rGO/polyacrylic acid (rGO/PAA), UV irradiation is used for the reduction of GO and polymerization PAA. The rGO/PAA composite film was synthesis with AA accounting for 10% wt., and UV radiation time of 3.6 seconds has the best electrochemical activity. Additionally, the effective area is 1.3 times larger than the geometric area. The composite film exhibits a specific capacitance (C_s) of 321 F/g at a current density of 1 A/g. Furthermore, the C_s value remains at 82% after 5000 charge-discharge cycles.

4. The fabrication of composite membranes comprising three constituents: rGO, polyaniline (PANi), and nanoMnO_2 by 3D printing and electrochemical deposition was investigated. Electrochemical analysis indicated the presence of 2% wt. MnO_2 nanoparticles have substantially enhanced the capacity of the rGO/PANi film. The C_s value of the composite rGO/PANi/MnO2 is 740 F/g at a current density of 1 A/g and retains 97% at a current density of 15 A/g after 5000 charge-discharge cycles.

5. The study focused on investigating RGO/poly (1,8-diaminonaphtalen) (P(1,8-DAN)) nano-transformers. The EDX, XPS, and FE-SEM spectral analyses confirmed the effective synthesis of the composite film rGO/P(1,8-DAN)/Ag, with an Ag content of 6.33% wt. It was found that rGO/P(1,8-DAN)/Ag electrodes produced linear signals for cefepime concentrations between 0.4 and 4 μM. The detection limit was found to be 0.08 μM, and the correlation factor was determined to be 0.993. Additionally, the relative standard deviation was calculated to be 2.2%. Analysis results of commercial electrode pharmaceutical samples with the potential to function as functional cefepime sensors.

LIST OF THE PUBLICATIONS RELATED TO THE DISSERTATION

1. Đỗ Thị Thủy, Lê Thị Mỹ Hạnh, Hoàng Trần Dũng, Đoàn Thanh Tùng, Lê Trọng Lư, Trần Đại Lâm, Nguyễn Tuấn Dung, Tổng hợp graphen oxit dạng gel ứng dụng làm mực in 3D, Tạp chí Hóa học, 2020, 58, 5E (1,2), 83-86.
2. Le T. M. Hanh, Do T. Thuy, Hoang T. Dung, Doan T. Tung, Vu X. Minh, Pham T. Lan, Le T. Lu, Tran D. Lam and Nguyen T. Dung, Development of Novel 3D printable graphene-based Composite Towards Fabrication of thin film electrode Material, Communication in Physics, 2020, 30(4), 383-390.
3. Đỗ Thị Thủy, Lê Thị Mỹ Hạnh, Hoàng Trần Dũng, Đoàn Thanh Tùng, Nguyễn Mạnh Tường, Trần Đại Lâm, Nguyễn Tuấn Dung, Ứng dụng kỹ thuật in 3D chế tạo điện cực màng mỏng trên cơ sở trên cơ sở composite graphen oxit/polyvinyl ancol, Tạp chí nghiên cứu khoa học và công nghệ quân sự, 2021, 74, 79-85.
4. Do Thi Thuy, Nguyen Tuan Dung, Tran Dai Lam, Hoang Tran Dung, Doan Thanh Tung, Le Thi My Hanh, Nguyen Huu Van, Synthesis thin film electrodes graphene via novel 3D printable technique and determine property electrochemical, Journal of Military Science and Technology, 2021, 75A, 29-37.
5. Nguyen Tuan Dung, Nguyen Le Huy, Do Thi Thuy, Bui Thi Hong Van, Nguyen Thi Tuyet Mai, Tran Dai Lam, Nguyen Tuan Dung, The role of copper decorating poly(1,8-diaminonaphthalene)/graphene electrode as a catalyst in the determination of nitrit, Vietnam Journal of Science and Technology, 2022, 60 (6), 1056-1066.
6. Thuy Thi Do, Hung Van Giap, Mai Tuyet Thi Nguyen, Dung Tran Hoang, Huy Le Nguyen, Lu Trong Le, Lam Dai Tran, Dzung Tuan Nguyen, 3D - printed layer-by-layer electrode graphene/poly(1,8-diaminonaphthalene) incorporated with silver nanoparticles as an electrochemical sensing platform for cefepime antibiotic determination, Colloid and Polymer Science, 2023, 301, 1029-1038 (SCIE, Q2, IF = 2,434).
7. Trong V. Vu, Mai. T.T. Nguyen, Thuy T. Do, Huy L. Nguyen, Vân-Anh Nguyen, Dzung T. Nguyen, Adsorption of Copper Ions onto Poly(1,8-diaminonaphthalene)/Graphene Film for Voltammetric Determination of Pyridoxine, Electroanalysis, 2022, 34(9), 1478-1486 (SCI, Q2, IF 3,223).

Đỗ Thị Thủy, Lê Thị Mỹ Hạnh, Đoàn Thanh Tùng, Hoàng Trần Dũng, Trần Đại Lâm, Lê Trọng Lư, Nguyễn Tuấn Dung, Sử dụng kết hợp kỹ thuật in 3D và lắng đọng điện hóa để chế tạo nanocomposite 3 thành phần rGO/PANi/MnO_2 làm vật liệu điện cực trong siêu tụ điện, Tạp chí Khoa học, Đại học Quốc Gia Hà Nội, đã có phản biện.